Nano Energy 34 (2017) 306–312

Contents lists available at ScienceDirect

Nano Energy

journal homepage: www.elsevier.com/locate/nanoen

Communication

Near-surface dilution of trace Pd atoms to facilitate Pd-H bond cleavage for giant enhancement of electrocatalytic hydrogen evolution

Yaping Li[a,1], Shuangming Chen[a,1], Ran Long[a,*], Huanxin Ju[a], Zhaowu Wang[b], Xiaoxi Yu[a], Fengyi Gao[a], Zijian Cai[a], Chengming Wang[a], Qian Xu[a], Jun Jiang[a], Junfa Zhu[a], Li Song[a,*], Yujie Xiong[a,*]

[a] Hefei National Laboratory for Physical Sciences at the Microscale, iChEM (Collaborative Innovation Center of Chemistry for Energy Materials), School of Chemistry and Materials Science, Hefei Science Center (CAS), and National Synchrotron Radiation Laboratory, University of Science and Technology of China, Hefei, Anhui 230026, PR China

[b] School of Physics and Engineering, Henan University of Science and Technology, Luoyang, Henan 471023, PR China

ARTICLE INFO

Keywords:
Near surface
Electrocatalysis
Hydrogen desorption
Lattice engineering
Hydrogen evolution reaction

ABSTRACT

Pd is a versatile catalyst in various hydrogen-related catalytic applications; however, it typically exhibits low activity in electrocatalytic hydrogen evolution reaction (HER) as too strong Pd-H bonding makes the electronic desorption of H adatoms (H_{ad}) hardly occur. We herein report a selective etching-deposition approach to implant trace Pd atoms in the near-surface region of Ag nanocrystals, forming a heteratomic-rich Pd-Ag structure on Ag surface. This near-surface dilution of Pd atoms can dramatically facilitate the electronic desorption of H_{ad}. As a result, this approach enhances the electrocatalytic HER activity of Pd catalysts about 14 times with excellent performance durability, approaching the high level of Pt catalysts. While enhancing the catalytic performance, this atomic implantation strategy allows the substantial reduction of material costs. This work thus represents a step toward the high-performance, low-cost catalyst design through near-surface lattice engineering.

1. Introduction

Pd is a noble metal catalyst that has been widely used for various hydrogen-related catalytic reactions due to its strong interaction with hydrogen [1,2]. In some catalytic applications, the hydrogen species eventually evolves as molecular hydrogen (H_2) so that the hydrogen adsorbed on Pd surface (i.e., H_{ad}) has to be released from Pd surface through desorption. In this case, too strong binding of H to Pd atoms often makes the H_{ad} desorption become the rate-limiting steps in catalytic processes [3–7]. For example, electrocatalytic hydrogen evolution reaction (HER, $2H^+ + 2e^- \rightarrow H_2$) is such a case that plays an important role in renewable hydrogen energy. The electronic desorption of H_{ad} from Pd surface can hardly occur, which makes Pd extremely inactive in HER with the activity typically 30–50 times lower than that of Pt [8–10]. As such, it would be highly important to maneuver the desorption of H_{ad} atoms through material design, overcoming this bottleneck.

Conceptually forming single-atom or few-atom Pd sites is a promising approach to weaken the binding of H to Pd [7,8]; The most straightforward approach is to deposit the Pd atoms on a substrate; however, the isolated metal atoms on supports often suffer from atomic migration/aggregation and catalyst deactivation [11–15]. Intuitively this limitation can be overcome by implanting Pd atoms in the substrate lattice of another metal [16]. On bare Pd surface, the H adsorption generally takes hollow sites [17], resulting in strong Pd-H bonding. When Pd atoms are diluted in the near-surface region of a metal lattice that has no binding with H atoms, it would be feasible to alter the adsorption configuration of H to Pd, facilitating the H_{ad} desorption. Meanwhile, the Pd atoms can be fixed in the lattice so as to reduce atomic mobility. In addition, confining Pd atoms in the near-surface region would also maximize the number of Pd atoms for surface catalysis, similarly to the atomic monolayer configuration [18,19].

In the selection of metal substrates, the chemical reactivity should be taken into account in terms of synthesis feasibility. Ideally a portion of near-surface atoms has to be removed to allow the implantation of Pd atoms while maintaining the matrix lattice. We thus choose Ag nanocrystals as a model system, as Ag atoms in surface lattice can be selectively etched to provide sites for Pd deposition but are not as

* Corresponding authors.
E-mail addresses: longran@ustc.edu.cn (R. Long), song2012@ustc.edu.cn (L. Song), yjxiong@ustc.edu.cn (Y. Xiong).
[1] Y. Li and S. Chen contributed equally.

http://dx.doi.org/10.1016/j.nanoen.2017.02.048
Received 21 December 2016; Received in revised form 22 February 2017; Accepted 25 February 2017
Available online 28 February 2017

susceptible to the air environment as other metals (e.g., Cu). Another merit is that the price of Ag is only 1/43 that of Pd, enabling significantly reducing material cost. In this report, we demonstrate a selective etching-deposition approach to implant trace Pd atoms (0.8 mol%) in the near-surface region of Ag nanocrystals, which can readily dilute Pd atoms in Ag near-surface lattice to form a heteratomic-rich Pd-Ag structure. Such atomic dilution provides an opportunity for tuning the adsorption of H to Pd toward a top-site configuration. As a result, the H_{ad} electronic desorption has been substantially facilitated for HER.

2. Experimental

2.1. Synthesis of Ag@PdAg nanocubes

In a standard procedure for Ag@PdAg nanocubes, 6.0 mL of an aqueous solution containing 0.5 mL of oleylamine, 1.0 mL of hydrochloric acid (2 M), 0.030*g* of L-ascorbic acid, 3.5 mL of ethylene glycol, and 1.0 mL of the aqueous suspension containing 1.6 mg of Ag nanocubes were mixed in a glass vial. The mixture was heated to 80 °C in air under magnetic stirring for 5 min. Meanwhile, 1.0 mL of an aqueous solution containing 3.0 mg of K_2PdCl_4 was added to the mixture by pipette under magnetic stirring. Heating of the reaction solution at 80 °C was continued in air for 20 min. The sample was washed with hexanol and then with ethanol three times to remove most of the oleylamine and other molecules by centrifugation.

2.2. Depth-dependent XPS characterization

X-ray photoelectron spectroscopy (XPS) experiments were performed at incident photon energies of 450, 550, and 600 at the Catalysis and Surface Science Endstation at the BL11U beamline in the National Synchrotron Radiation Laboratory (NSRL) in Hefei, China. The photon energies were calibrated using the bulk Au $4f_{7/2}$ core level located at 84.0 eV as the reference. The Ag 3d and Pd 3d spectra were normalized by the beam flux and the photoionization cross-section factors, while the atomic fraction was calculated after subtraction of a Shirley background.

2.3. XAFS characterization

Pd and Ag *K*-edge X-ray absorption fine structure (XAFS) measurements were made at the beamline 14W1 in Shanghai Synchrotron Radiation Facility (SSRF), China. The X-ray was monochromatized by a double-crystal Si(311) monochromator. The storage ring of SSRF was operated at 3.5 GeV with the current of 300 mA. The acquired extended XAFS (EXAFS) data were processed according to the standard procedures using the WinXAS3.1 program. Theoretical amplitudes and phase-shift functions were calculated with the FEFF8.2 code using the crystal structural parameters of the Ag foil, PdO and Pd foil. X-ray absorption near-edge structure (XANES) calculation was based on self-consistent multiple-scattering (MS) methods, and was carried out using the FEFF8.2 code. For the exchange correlation part of the potential, the Hedin-Lundqvist (H-L) model was employed.

2.4. Electrocatalytic HER measurement

All the electrochemical measurements were performed in a three-electrode system on an electrochemical workstation (CHI 760E, Shanghai Chenhua, China) in 0.5-M H_2SO_4 electrolyte. The catalysts dispersed onto a glassy carbon rotating disk electrode (GC RDE, PINE, PA, USA) were used as a working electrode, while a reversible hydrogen electrode (RHE) and a platinum foil served as the reference and counter electrodes, respectively. The GC RDE has a diameter of 5 mm and a geometric area of 0.19625 cm^2. The electrode was firstly polished with emery paper of decreasing grades and then with Al_2O_3 powders with size down to 0.05 μm. Prior to the deposition of catalysts, the electrode was immersed in ethanol and then thoroughly rinsed with DI water three times to remove contaminants. To prepare the working electrode, 18 μL of an aqueous suspension containing 80-μg catalysts was transferred to the GC RDE. No supports were used for the catalysts in our electrocatalytic measurements. Commercial Pd/C catalysts (Sigma-Aldrich, Pd: 10% wt.) were used as a reference to evaluate the electrocatalytic performance of various samples. The metal loading weights for all the samples were kept consistent. Prior to electrocatalytic measurements, the working electrode was cleaned with RF plasma (Plasma Cleaner pdc-002, Harrick, NY, USA) at a power level of 10.5 W for 1.5 min to remove residue organics, and then covered with 10 μL of Nafion dispersed in water (0.025%). Linear sweep voltammetry with a scan rate of 2 mV s^{-1} was conducted with a flow of Ar gas maintained over the electrolyte during the HER experiment to eliminate dissolved oxygen. The working electrode was rotated at 1600 rpm to remove hydrogen gas bubbles formed at the catalyst surface. Cyclic voltammetry (CV) was conducted between −0.3 and 0.1 V versus RHE at 50 mV s^{-1} for 5000 times to investigate the cycling stability. 5 independent measurements were performed to confirm the consistency of data. We used 90% of the values for *iR* corrections, in order to reduce the negative impacts from the system resistance and adsorption processes.

2.5. First-principles simulation

Density functional theory (DFT) simulations were performed with the Vienna *ab* initio simulation (VASP) package. Perdew-Burke-Ernzerhof (PBE) exchange-correlation functional within a generalized gradient approximation (GGA) and the projector augmented-wave (PAW) potential were employed. The metal surface was modeled with 3×3 slab with four layers, and the vacuum region was set to 15 Å. Two bottom layers of the four layers were fixed to the bulk positions during the relaxation. Gamma centered k-points grid of 4×4×1 is used for the supercell. The simulation supercell is fully relaxed to obtain the ground state with a force convergence < 0.01 eV/Å. Three adsorption configurations, bridge-, hollow- and top-sites were considered to obtain the most favorable one. The adsorption of H atom on Pd(100) surface and Pd-implanted Ag(100) surface was analyzed based on the most favorable adsorption configurations.

3. Results and discussion

In the implantation of Pd atoms in the near-surface region of Ag nanocrystals, the most challenging task is to suppress the galvanic replacement of Ag nanocrystals with Pd precursor. The galvanic replacement would substantially etch the template of Ag nanocrystals and consume the Pd precursor [20,21], which forms a huge obstacle for selectively implanting trace Pd atoms in the near-surface region of Ag nanocrystals. Adding a reducing agent such as ascorbic acid, which induces the reduction of Pd and Ag ions, can suppress the replacement to some extent; however, the co-deposition of Pd and Ag atoms together with the remaining galvanic replacement would result in high Pd-to-Ag ratios on surface [21]. For this reason, we decide to employ oleylamine as a capping agent, which has strong binding to metal surface [22], to cover the surface of Ag nanocrystals so as to largely suppress the galvanic replacement.

Our synthesis is thus based on the template of cubic Ag nanocrystals with the average edge length of 58 nm (Fig. S1) prepared by following our previous protocol [23]. To implant Pd atoms in the near-surface region of Ag nanocrystals, the Ag nanocubes are treated by the combination of oleylamine and hydrochloric acid (HCl), with the addition of K_2PdCl_4 as a Pd precursor and ascorbic acid as a reducing agent in the presence of O_2. As the surface of Ag nanocubes is protected by oleylamine, the Ag surface becomes relatively passivated against oxidation. Previous research indicates that a corrosive pitting process

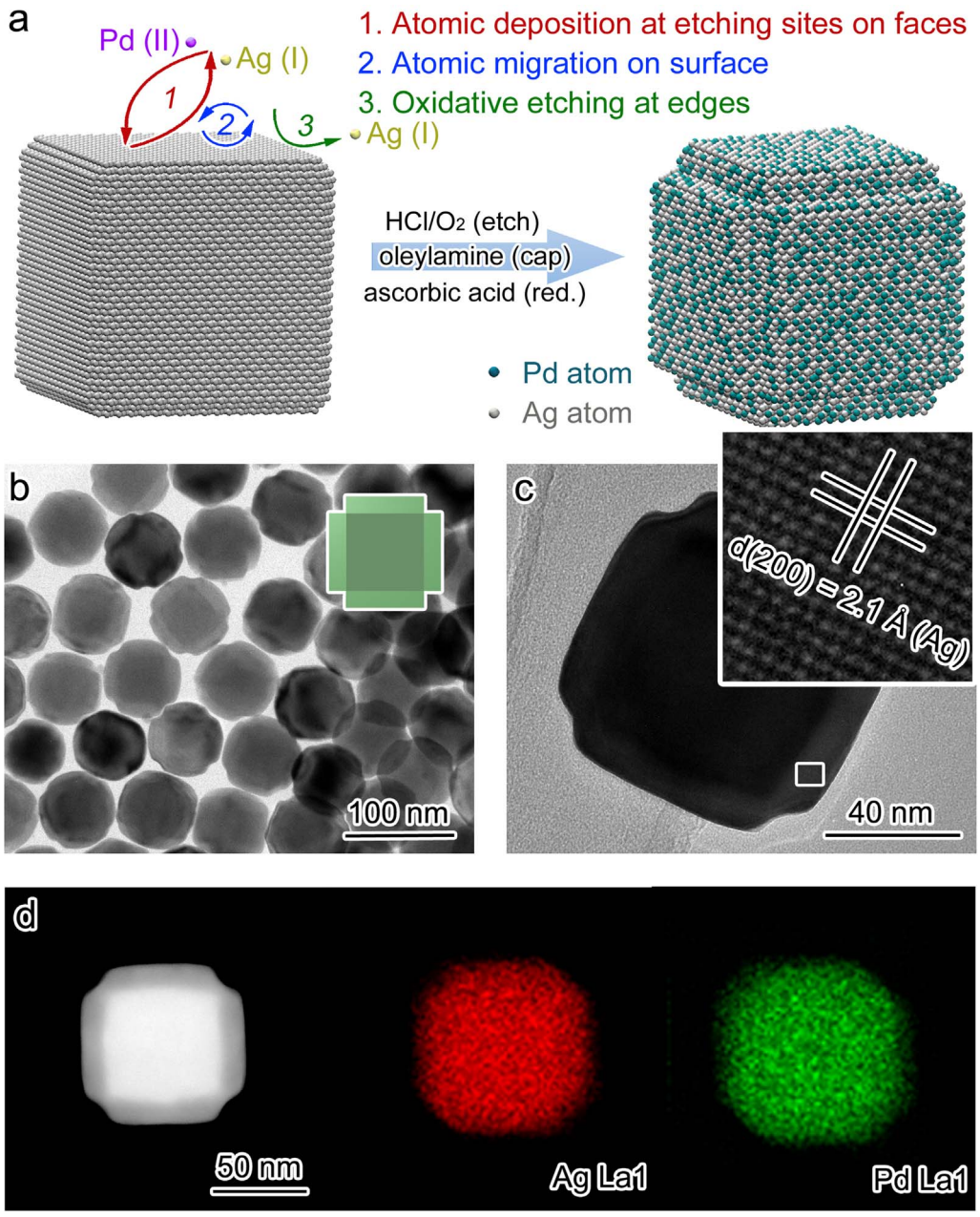

Fig. 1. (a) Schematic illustration for implanting trace Pd atoms in the near-surface region of Ag nanocrystals during the synthetic process. (b) TEM and (c) high-resolution TEM images of the Ag@PdAg nanocubes obtained from the synthesis in panel a. (d) HAADF-STEM image and EDS mapping profiles (green, Pd; red, Ag) of a Ag@PdAg nanocube.

can take place on surface when metal nanocrystals are covered by excessive capping agents [24]. In our case, O_2/HCl pair is used as an effective etchant [23] to initiate an oxidative etching process. Given the passivated surface, the oxidative etching by O_2 and HCl can remove only a small number of Ag atoms from the surface. Most likely, the galvanic replacement with K_2PdCl_4 may simultaneously make a contribution to the removal of trace surface Ag atoms although this process has been greatly suppressed by oleylamine protection. The removal of trace Ag atoms from surface provides sites for the deposition of Pd atoms when the K_2PdCl_4 is reduced by ascorbic acid, implanting the Pd atoms in the lattice of Ag surface (Fig. 1a, Process 1). The incorporated Pd atoms will undergo atomic migration on surface and diffusion into lattice to form a stable structure in the near-surface region (Fig. 1a, Process 2) [25,26].

Fig. 1b and S2 display the transmission electron microscopy (TEM) images of the sample after the selective etching-deposition process. By implementing the process, the lateral dimension of nanocrystals can be well maintained while the original edges of Ag nanocubes have been partially removed. It suggests that more intensive oxidative etching occurs at the edges (Fig. 1a, Process 3), due to the higher reactivity of edge atoms. It turns out that both oleylamine capping and HCl-enhanced etching are crucial to the selective etching-deposition process (Figs. S3 and S4). Only with full surface coverage by oleylamine, the galvanic replacement can be substantially suppressed, and the oxidative etching by O_2/HCl can remove a certain number of Ag atoms to make them accessible for the incorporation of Pd atoms into near-surface lattice. Thus the capping and etching effects should be balanced to achieve our designed synthesis. In addition, such a selective etching-deposition synthetic scheme can also be extended to other metals such as the deposition of Pd atoms on Cu nanocubes (Fig. S5), despite the relatively low quality of Cu template.

Upon the completion of designed synthesis, the next question would be whether the Pd atoms are truly implanted in the near-surface region of Ag nanocubes. X-ray diffraction (XRD) suggests that the Ag

matrix lattice has not been altered (Fig. S6), which is further supported by high-resolution TEM (Fig. 1c). Despite the removal of edges by oxidative etching, the lattice near the edges of Ag nanocubes is well maintained. The lattice fringes assigned to Ag(200) reveal that the nanocrystals are bounded by {100} facets. To resolve the spatial distribution of Pd and Ag, we have collected energy-dispersive spectroscopy (EDS) mapping profiles on aberration-corrected high-angle annular dark-field scanning TEM (HAADF-STEM, Fig. 1d), indicating that the Pd is deposited on the surface of Ag nanocubes. As the *L* line energies for Pd and Ag elements are quite close, it is not highly reliable to provide contrast for distinguishing Pd from Ag.

To confirm the presence of Pd in Ag lattice, we have measured chemical compositions using inductively-coupled plasma mass spectrometry (ICP-MS). The ICP-MS data show that the content of Pd is 0.8 mol% in the formed nanostructures. Given the average edge length of 58 nm, the surface atoms of a cubic nanocrystal should account for about 1.7% of the total atoms (see Supporting Note 1). Thus the Pd atoms in the product cannot fully cover the surface of nanocubes. In this case, the structure should be an edge-etched Ag nanocube with an ultrathin PdAg alloy surface (namely, Ag@PdAg nanocubes).

To prove this feature, depth-dependent XPS has been performed using a synchrotron radiation technique at incident photon energies of 450, 550, and 600 eV, providing information for vertical elemental distribution. As estimated by the XPS data [27], the average Pd atomic fractions in our Ag@PdAg nanocubes decrease from 0.098 to 0.074 as the depths are extended from ~0.8 nm (hv=450 eV) to ~1.0 nm (hv=600 eV) (Fig. 2a) [28]. We can thus conclude that the Pd atoms are mostly distributed in the near-surface region of nanocrystals at a low concentration. To demonstrate the niche of our synthetic strategy, we have followed the standard protocol in literature [21], in which galvanic replacement still takes place to alloy the Ag and Pd, to make a reference sample (Fig. S7). As reported in literature [21], the reference sample contains the Pd content of 2.2–7.3% (*versus* 0.8% in our Ag@PdAg nanocubes), and possesses 2–5 layers of PdAg alloy in the shells (namely, Ag@PdAg-ref nanocubes). As indicated by the XPS, the Ag@PdAg-ref nanocubes possess significantly higher Pd atomic fractions, ranging from 0.318 for 0.8-nm depth to 0.259 for 1.0-nm depth (Fig. 2b).

Given the ultralow concentration of Pd atoms, it is imperative to precisely resolve the local structural information for Pd and Ag atoms. Apparently XRD is not sufficiently sensitive to detect the structural changes induced by the ultralow concentration of Pd atoms at 0.8%. For this reason, the samples are characterized by synchrotron radiation-based XAFS spectroscopy. Figs. S8 and S9 show the Pd and Ag *K*-edge EXAFS spectra processed through a Fourier-transform (FT) (Fig. S10), using standard Pd and Ag foils as the references. The reduced amplitude and slight phase shifts in the Pd *K*-edge spectra of Ag@PdAg and Ag@PdAg-ref nanocubes (Fig. S8) indicate that Pd atoms exist in the alloyed outer surface. In particular, the major peak at 2.57 Å for the 1st shell of Pd in Ag@PdAg is distinctly red-shifted as compared with Pd standard (2.47 Å), indicating the formation of bimetallic alloy at surface. In comparison, the Ag *K*-edge spectra do not show distinct difference in terms of phase and amplitude (Fig. S9) as the Ag atoms detected by EXAFS are mostly internal in the Ag@PdAg and Ag@PdAg-ref samples. The local structure around Ag atoms shows indistinct changes as compared with Ag standard, indicating that the Ag atoms mainly retain the original Ag lattice.

To look into bonding situation, we extracted metal-metal bond lengths and metal coordination numbers (CNs) from EXAFS curve fitting. It is known that the CNs of atoms inside a face-centered cubic (*fcc*) lattice and on its faces are 12 and 8, respectively. As listed in Table 1, the total CN of Pd (i.e., $CN_{Pd-Ag}+CN_{Pd-Pd}$) in our Ag@PdAg

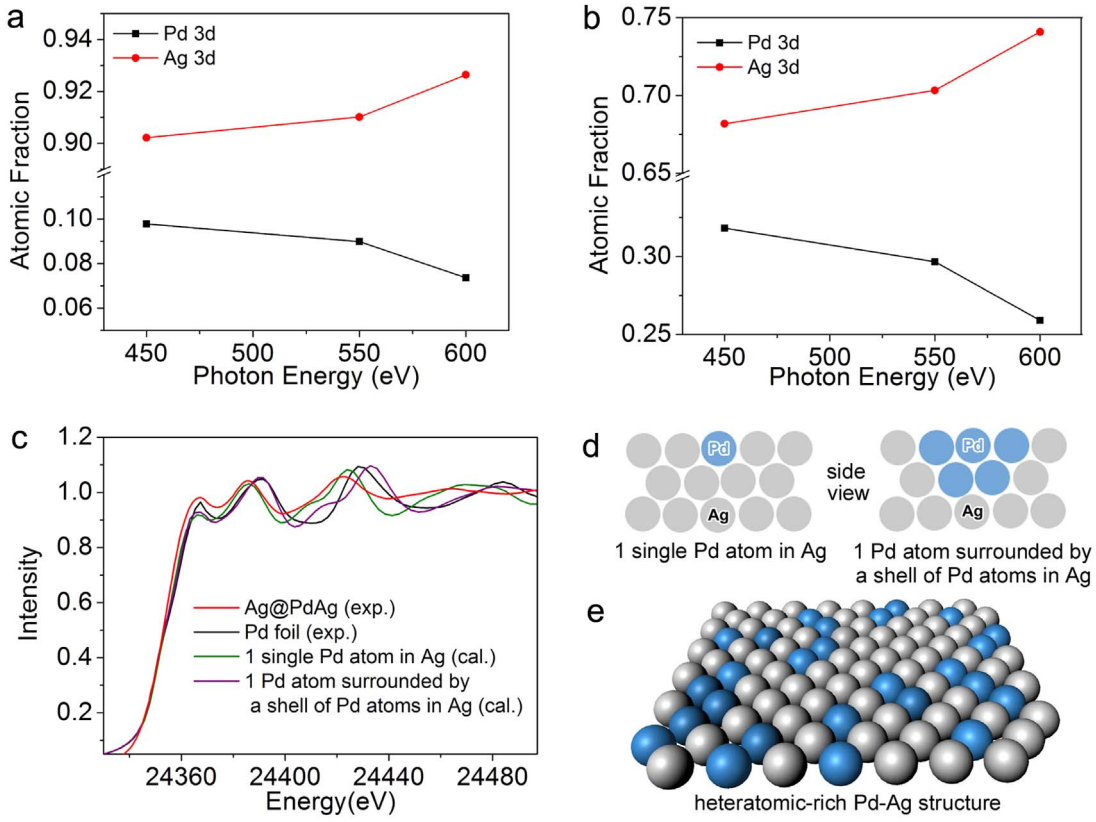

Fig. 2. Dependence of Pd and Ag atomic fractions of (a) the obtained Ag@PdAg nanocubes and (b) the Ag@PdAg-ref nanocubes prepared by following the literature protocol [21], measured by XPS as a function of photon energy. (c) The comparison between the experimentally collected Pd *K*-edge XANES spectra (Ag@PdAg nanocubes, and Pd foil) and the calculated spectra (1 single Pd atom in Ag, and 1 Pd atom surrounded by a shell of Pd atoms in Ag). (d) Models for XANES calculation. (e) Schematic illustration for heteratomic-rich Pd-Ag surface.

Table 1
Fitting results of Ag and Pd *K*-edge EXAFS data. The lengths of Ag-Ag, Ag-Pd, Pd-Ag, Pd-Pd and Pd-O bonds and coordination numbers of Ag and Pd atoms were extracted from the curve-fitting for Ag and Pd *K*-edge EXAFS data (Figs. S8 and S9), respectively. R, the lengths of Ag-Ag, Pd-Pd and Pd-Ag bonds; CN, the coordination numbers of Ag and Pd atoms; σ^2, the Debye-Waller factor. Error bounds (accuracies) are estimated as CN, ± 5%; R, ± 1%; σ^2, ± 1%.

Sample	EXAFS	Bond	R (Å)	CN	σ^2 (10^{-3} Å^2)
Ag@PdAg	Ag *K*	Ag-Ag	2.86	11.2	9.8
		Ag-Pd	2.87	0.6	11.4
	Pd *K*	Pd-Ag	2.87	5.3	11.4
		Pd-Pd	2.79	3.2	6.5
		Pd-O	2.12	1.6	2.1
Ag@PdAg-ref	Ag *K*	Ag-Ag	2.86	8.7	9.7
		Ag-Pd	2.81	3.2	10.5
	Pd *K*	Pd-Ag	2.81	4.5	10.5
		Pd-Pd	2.79	4.2	8.7
		Pd-O	2.00	0.8	2.3
Ag foil	Ag *K*	Ag-Ag	2.86	12.0	9.6
Pd foil	Pd *K*	Pd-Pd	2.74	12.0	5.8

sample is 8.5, indicating that Pd atoms are mostly located in the first-layer surface of nanocrystals. Moreover, the CN of Pd-Ag bond is much higher than the CN of Pd-Pd bond (5.3 for Pd-Ag *versus* 3.2 for Pd-Pd), suggesting that Pd atoms are well separated as single-atom or few-atom sites in the outermost layer. In comparison, the Pd atoms in the sample obtained from the conventional method (i.e., Ag@PdAg-ref) are more aggregated according to the CN_{Pd-Pd} of 4.2. More importantly, the Ag *K*-edge EXAFS data reveals that more Pd atoms are immersed in bulk Ag lattice in the Ag@PdAg-ref sample, as indicated by the CN_{Ag-Pd} comparison (3.2 for Ag@PdAg-ref *versus* 0.6 for Ag@PdAg).

To better resolve the local structure of Pd atoms, we have reproduced the Pd *K*-edge XANES features by means of multiple scattering theory (Fig. 2c). In the calculation, two models are used to represent the status of "isolation of single Pd atoms in the near-surface region of Ag nanocrystals" *versus* "confinement of contiguous Pd atoms in the near-surface region of Ag nanocrystals". The single Pd atom in the model of "1 single Pd atom in Ag" is fully surrounded by Ag atoms, while the model of "1 Pd atom surrounded by a shell of Pd atoms in Ag" contains a full shell of Pd atoms (Fig. 2d). The comparison (Fig. 2c) shows that the spectrum experimentally collected for our Ag@PdAg sample is more consistent with the calculation result for "1 single Pd atom in Ag", indicating that the Pd atoms are largely separated by Ag atoms (i.e., the "heteratomic-rich Pd-Ag structures", Fig. 2e) [29]. Certainly we cannot completely exclude the possibility that there may exist few contiguous Pd atoms, but the Pd atoms are absolutely not all contiguous over the surface of Ag nanocrystals. Thus our synthetic approach has the advantage of implanting trace Pd atoms in the near-surface region of Ag nanocrystals to form heteratomic-rich Pd-Ag structures, achieving our design for facilitating Pd-H cleavage. In sharp contrast, the conventional catalysts such as Pd-Ag alloys have Pd atoms distributed in entire particles no matter how diluted the concentrations of Pd atoms are. Given that the Pd atoms in bulk cannot participate in catalysis, our synthetic scheme offers a unique approach to reduce the Pd usage in catalysts, which cannot be replaced by other techniques.

We are now in a position to investigate the efficacy of near-surface atomic dilution in the enhancement of electrocatalytic HER, using bare Pd nanocubes with comparable edge lengths (Fig. S11) as a reference sample. Fig. 3a shows the HER polarization curves for all the samples in reference to commercial Pd/C at the same metal loading weight of 0.08 mg. Strikingly our Ag@PdAg nanocubes exhibit dramatically higher electrocatalytic activity as compared with their counterpart nanostructures and commercial Pd/C. The Ag@PdAg nanocubes offer a current density of 382 mA cm^{-2} at −0.3 V, comparable to that of Pt catalysts [19], with the Tafel slope down to 70 mV dec^{-1} (Fig. 3b). In literature [19], the mass specific activity of Pt monolayer – a configuration for maximal atomic utilization is 8.3×10^4 A/g_{Pt} at −0.3 V. Thus the mass specific activity of 11.9×10^4 A/g_{Pd} here manifests the HER activity approaching the high level of Pt catalysts. We have also compared the performance with those for Pd-based nanostructures in literature based on the values of current density and catalyst usage. The mass specific activities by the reported $PdCu_3$ and PdPS are about 2.2×10^3 A/g_{Pd} and 7.6×10^2 A/g_{Pd} at −0.2 V, respectively [30,31], while our Ag@PdAg nanocubes offer a mass specific activity of 3.3×10^4 A/g_{Pd} at −0.2 V. The high mass specific activity of our sample is enabled by the maximal usage of Pd atoms on surface. As a reference, the Tafel slopes of Pd/C, Pd nanocubes and Ag nanocubes are 108, 123, and 134 mV dec^{-1}, respectively, in agreement with the reported value in literature [9].

The Tafel slope is an indicator for the rate-determining reactions [32], and as such, the reduced slope suggests that the HER process has been maneuvered by diluting Pd atoms in Ag matrix. As a matter of fact, the Ag@PdAg-ref sample with the surface Pd atoms more concentrated also exhibits a Tafel slope reduction to 83 mV dec^{-1}. In principle, the HER in acidic medium involves a primary discharge step (i.e., Volmer step) and two electronic desorption steps (i.e., Heyrovsky step and Tafel step) [32]. The ideal Tafel slopes are 120, 40, and 30 mV decade^{-1} when the Volmer, Heyrovsky, and Tafel steps determine the rate, respectively. The large Tafel slopes of Pd nanocubes and Pd/C catalysts indicate that the electronic desorption of H_{ad} from the Pd surface can hardly occur [32]. Thus Heyrovsky or/and Tafel steps should be the rate-limiting steps, as commonly noted in literature [9]. As indicated by the reduction of Tafel slopes from 123 to 70 mV decade^{-1}, our atomic dilution strategy has substantially facilitated the electronic desorption steps — Heyrovsky or/and Tafel steps. As a result, the HER current density has been dramatically improved from 28 to 382 mA cm^{-2} at −0.3 V with the enhancement factor of about 14 times.

Another key parameter is the overpotential indicating the required electron energy for HER [33]. As shown in Fig. 3c, the overpotentials of samples follow the order of Ag nanocubes > commercial Pd/C > Pd nanocubes > Ag@PdAg-ref nanocubes > Ag@PdAg nanocubes. The overpotentials of Ag@PdAg are 20.3 mV at 1 mA cm^{-2} and 93.0 mV at 10 mA cm^{-2}, respectively, comparable to the values for excellent Pd-based catalysts in literature [30,31]. It again manifests that the electrochemical desorption of H atom from the diluted Pd atoms can easily take place. This finding is consistent with the trend of onset potentials, in which the small onset potential of 13.8 mV for Ag@PdAg indicates that reduction reaction can smoothly occur [33]. It is worth noting that negligible decay in the HER activity can be observed for our Ag@PdAg nanocubes between the curves measured at the initial cycle and after 5000 CV cycles (Fig. 3d), suggesting the excellent durability during long-term cycling. TEM image (Fig. S12) shows that the morphology of Ag@PdAg nanocubes is largely maintained after the HER reaction, which can be responsible for the excellent durability.

To gain insight into the tunable H_{ad} desorption with Pd atomic separation, we have employed first-principles simulations to examine the H adsorption and desorption on Pd surface. We have calculated the absorption energies of H atoms on Pd in three possible configurations including bridge-, hollow-, and top-sites, using two substrates – Pd(100) surface and Pd-implanted Ag(100) surface as simulation models. In order to simplify the case, an extreme model that a single Pd atom is completely surrounded by Ag is used to represent our heteratomic-rich Pd-Ag structure. According to the adsorption energies, the most favorable adsorption configuration for Pd(100) facet is to chemisorb the H atom at the hollow site confined by four neighbored Pd atoms, with an adsorption energy of −3.78 eV. In sharp contrast, as the Pd atom is separated by Ag atoms, the most favorable adsorption configuration is altered to the top site of Pd atom (Fig. S13). Such a change in adsorption configuration significantly reduces the adsorption

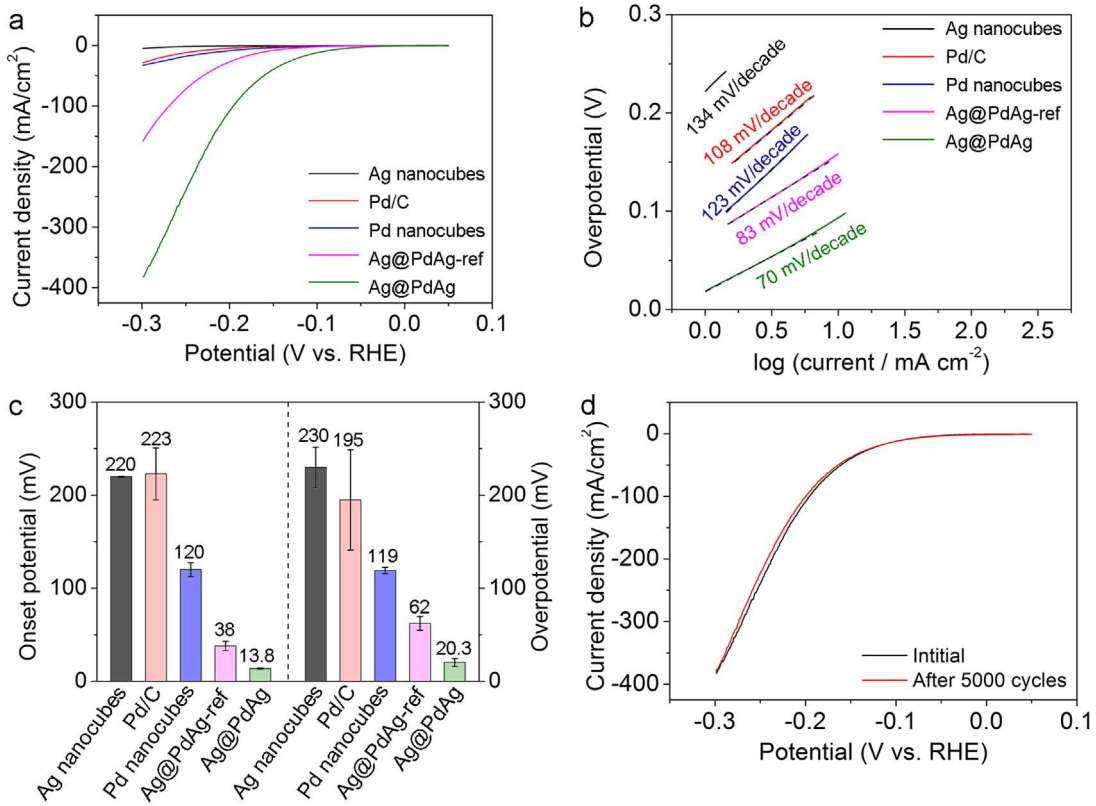

Fig. 3. (a) Polarization curves, (b) corresponding Tafel plots, and (c) onset potentials and overpotentials obtained on glassy carbon rotating disk electrodes coated with Ag@PdAg nanocubes and Ag@PdAg-ref nanocubes for electrocatalytic HER in an Ar-saturated 0.5-M H_2SO_4 solution, in reference to commercial Pd/C, Ag nanocubes, and Pd nanocubes, the error bars from the 5 independent measurements. 5 independent measurements have been performed to confirm the high consistency of data. (d) Durability test of our Ag@PdAg nanocubes for 5000 cycles from −0.3 to 0.1 V at 50 mV s^{-1}.

energy to −3.18 eV (Table S1). The essence of adsorption energy variation is caused by the reduced number of H-bonded Pd atoms from 4 to 1, associated with the adsorption configurations. To reflect the hydrogen evolution process, we have also obtained the energy values for the desorption process of H_{ad} atom from Pd(100) surface and Pd-implanted Ag(100) surface to form H_2 (Table S2), which depict the energy evolution from the adsorbed H atoms to free H_2 molecules. The simulation indicates that the energy evolution for the desorption of H_{ad} atom from Pd-implanted Ag(100) surface is −0.18 eV while that for Pd(100) surface is 0.43 eV. The exothermic process of H_{ad} desorption to form H_2 shows that HER can more easily take place on Pd-implanted Ag(100). Specifically, the HER is promoted by facilitating the electronic desorption steps.

4. Conclusion

In conclusion, we have designed the Pd-implanted Ag nanostructures through a selective etching-deposition approach. The dilution of trace Pd atoms in the near-surface region of Ag nanocrystals, which has been unambiguously resolved by synchrotron-radiation characterizations, can alter the adsorption of H atoms from hollow- to top-sites. As a result, the Pd-H bond cleavage can be facilitated to dramatically enhance HER activity. Notably the electrocatalytic HER performance has been improved about 14 times as compared with conventional Pd catalysts, approaching the high level of Pt catalysts. This giant HER enhancement overcomes the long-standing bottleneck of Pd catalysts in HER, and provides an alternative strategy for engineering catalytic materials toward hydrogen-related applications. Given the low cost of Ag matrix material and the ultralow usage of Pd atoms (0.8 mol% Pd in catalysts), the cost of our Ag@PdAg catalyst is only $24.11/pound based on the current metal prices in Table S3, about 3.1% that of Pd and 2.4% that of Pt. More importantly, the Pd atoms in our catalyst are confined in the near-surface region, which boosts the utilization of Pd atoms in electrocatalytic HER. As such, the required usage of catalyst can be reduced by our design as compared with conventional Pd-based alloy catalysts. The concept demonstrated here calls for future efforts on near-surface lattice engineering at atomic precision for high-performance and low-cost electrocatalyst design.

Acknowledgements

This work was financially supported in part by 973 Program (No. 2014CB848900), NSFC (No. 21471141, U1532135, 21601173, 21573212, 11404095), CAS Key Research Program of Frontier Sciences (QYZDB-SSW-SLH018), Recruitment Program of Global Experts, CAS Hundred Talent Program, Hefei Science Center CAS (2015HSC-UP009), Anhui Provincial Natural Science Foundation (1608085QB24, 1508085MB24), and China Postdoctoral Science Foundation (2015T80660). Depth-dependent XPS experiments were performed at the Catalysis and Surface Science Endstation in the National Synchrotron Radiation Laboratory (NSRL) in Hefei, China. EXAFS measurements were performed at the beamline BL14W1 in the Shanghai Synchrotron Radiation Facility (SSRF), China.

Appendix A. Supporting information

Supplementary data associated with this article can be found in the online version at doi:10.1016/j.nanoen.2017.02.048.

References

[1] Y. Wang, J. Yao, H. Li, D. Su, M. Antonietti, J. Am. Chem. Soc. 133 (2011) 2362–2365.
[2] K. Tedsree, T. Li, S. Jones, C.W. Chan, K.M. Yu, P.A. Bagot, E.A. Marquis, G.D. Smith, S.C. Tsang, Nat. Nanotechnol. 6 (2011) 302–307.

[3] A. Maiti, R. Gee, R. Maxwell, A. Saab, J. Phys. Chem. B 110 (2006) 3499–3503.
[4] M. Blanco-Rey, J.I. Juaristi, R. Diez Muino, H.F. Busnengo, G.J. Kroes, M. Alducin, Phys. Rev. Lett. 112 (2014) 103203.
[5] W. Dong, Phys. Rev. B 56 (1997) 15396–15403.
[6] Y. Dai, X. Mu, Y. Tan, K. Lin, Z. Yang, N. Zheng, G. Fu, J. Am. Chem. Soc. 134 (2012) 7073–7080.
[7] G. Kyriakou, M.B. Boucher, A.D. Jewell, E.A. Lewis, T.J. Lawton, A.E. Baber, H.L. Tierney, M. Flytzani-Stephanopoulos, E.C. Sykes, Science 335 (2012) 1209–1212.
[8] Z. Fan, Z. Luo, X. Huang, B. Li, Y. Chen, J. Wang, Y. Hu, H. Zhang, J. Am. Chem. Soc. 138 (2016) 1414–1419.
[9] J. Durst, C. Simon, F. Hasche, H.A. Gasteiger, J. Electrochem. Soc. 162 (2015) F190–F203.
[10] P. Quaino, E. Santos, Langmuir 31 (2015) 858–867.
[11] X.F. Yang, A. Wang, B. Qiao, J. Li, J. Liu, T. Zhang, Acc. Chem. Res. 46 (2013) 1740–1748.
[12] J. Jones, H. Xiong, A.T. DeLaRiva, E.J. Peterson, H. Pham, S.R. Challa, G. Qi, S. Oh, M.H. Wiebenga, X.I. Pereira Hernandez, Y. Wang, A.K. Datye, Science 8 (2016) 150–154.
[13] M. Moses-DeBusk, M. Yoon, L.F. Allard, D.R. Mullins, Z. Wu, X. Yang, G. Veith, G.M. Stocks, C.K. Narula, J. Am. Chem. Soc. 135 (2013) 12634–12645.
[14] B. Qiao, A. Wang, X. Yang, L.F. Allard, Z. Jiang, Y. Cui, J. Liu, J. Li, T. Zhang, Nat. Chem. 3 (2011) 634–641.
[15] H. Yan, H. Cheng, H. Yi, Y. Lin, T. Yao, C. Wang, J. Li, S. Wei, J. Lu, J. Am. Chem. Soc. 137 (2015) 10484–10487.
[16] N. Becknell, Y. Kang, C. Chen, J. Resasco, N. Kornienko, J. Guo, N.M. Markovic, G.A. Somorjai, V.R. Stamenkovic, P. Yang, J. Am. Chem. Soc. 137 (2015) 15817–15824.
[17] R. Long, Z. Rao, K. Mao, Y. Li, C. Zhang, Q. Liu, C. Wang, Z.Y. Li, X. Wu, Y. Xiong, Angew. Chem. Int. Ed. 54 (2014) 2425–2430.
[18] D.V. Esposito, S.T. Hunt, A.L. Stottlemyer, K.D. Dobson, B.E. McCandless, R.W. Birkmire, J.G. Chen, Angew. Chem. Int. Ed. 49 (2010) 9859–9862.
[19] M. Li, Q. Ma, W. Zi, X. Liu, X. Zhu, S.F. Liu, Sci. Adv. 1 (2015) e1400268.
[20] J. Chen, B. Wiley, J. McLellan, Y. Xiong, Z.Y. Li, Y. Xia, Nano Lett. 5 (2005) 2058–2062.
[21] J. Li, J. Liu, Y. Yang, D. Qin, J. Am. Chem. Soc. 137 (2015) 7039–7042.
[22] Z. Niu, Q. Peng, M. Gong, H. Rong, Y. Li, Angew. Chem. Int. Ed. 50 (2011) 6315–6319.
[23] B. Li, R. Long, X. Zhong, Y. Bai, Z. Zhu, X. Zhang, M. Zhi, J. He, C. Wang, Z.Y. Li, Y. Xiong, Small 8 (2012) 1710–1716.
[24] Y. Xiong, B. Wiley, J. Chen, Z.Y. Li, Y. Yin, Y. Xia, Angew. Chem. Int. Ed. 44 (2005) 7913–7917.
[25] N.P. Dasgupta, C. Liu, S. Andrews, F.B. Prinz, P. Yang, J. Am. Chem. Soc. 135 (2013) 12932–12935.
[26] X. Xia, S. Xie, M. Liu, H.C. Peng, N. Lu, J. Wang, M.J. Kim, Y. Xia, Proc. Natl. Acad. Sci. USA 110 (2013) 6669–6673.
[27] F. Tao, M.E. Grass, Y. Zhang, D.R. Butcher, J.R. Renzas, Z. Liu, J.Y. Chung, B.S. Mun, M. Salmeron, G.A. Somorjai, Science 322 (2008) 932–934.
[28] C.J. Powell, A. Jablonski, National Institute of Standards and Technology, Gaithersburg, 2000.
[29] B.J. Hwang, L.S. Sarma, J.M. Chen, C.H. Chen, S.C. Shih, G.R. Wang, D.G. Liu, J.F. Lee, M.T. Tang, J. Am. Chem. Soc. 127 (2005) 11140–11145.
[30] S. Sarkar, S. Sampath, Chem. Commun. 50 (2014) 7359–7362.
[31] R. Jana, A. Bhim, P. Bothra, S.K. Pati, S.C. Peter, ChemSusChem 9 (2016) 2922–2927.
[32] T. Shinagawa, A.T. Garcia-Esparza, K. Takanabe, Sci. Rep. 5 (2015) 13801.
[33] H.B. Wu, B.Y. Xia, L. Yu, X.Y. Yu, X.W. Lou, Nat. Commun. 6 (2015) 6512.

Yaping Li received her B.S. degree in Applied Chemistry from the Central South University in 2013. She is currently a Ph.D. student under the tutelage of Professor Yujie Xiong at the University of Science and Technology of China (USTC). Her research interests focus on metal nanostructures and electrocatalysis.

Shuangming Chen received his Ph.D. degree from National Synchrotron Radiation Laboratory (NSRL), University of Science and Technology of China (USTC). He is currently a postdoctoral fellow working with Professor Li Song at the USTC. His research is mainly focusing on in-situ and ex-situ SR-related investigations of noble metal nanoparticles, 2D nanomaterials and their hybrids.

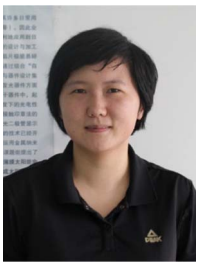

Ran Long received her B.S. in chemistry in 2009 and Ph.D. in inorganic chemistry under the tutelage of Professor Yujie Xiong in 2014, both from the University of Science and Technology of China (USTC). She is currently a Research Associate Professor at the USTC. Her research interests focus on controlled synthesis and catalytic applications of metal nanocrystals.

Li Song received his Ph.D. degree from Institute of Physics, Chinese Academy of Sciences. Currently, he is a professor in National Synchrotron Radiation Laboratory (NSRL), University of Science and Technology of China (USTC). His research interests include low-dimensional nanocarbons, 2D layered quantum nanostructures and their applications for nanodevice and clean energy.

Yujie Xiong received his B.S. in chemical physics in 2000 and Ph.D. in inorganic chemistry under the tutelage of Professor Yi Xie in 2004, both from the University of Science and Technology of China (USTC). After four-year training with Professors Younan Xia and John A. Rogers, he joined the National Nanotechnology Infrastructure Network (NSF-NNIN), and served as the Principal Scientist and Lab Manager at Washington University in St. Louis. In 2011, he moved to the USTC to take the position of Professor of Chemistry. His research interests include synthesis, fabrication and assembly of inorganic materials for energy and environmental applications.